

New Insights in the Primary Breakup Process of Prefilming Airblast Atomizers by SPH Predictions

S. Holz*, S. Braun, G. Chaussonnet, T. Dauch, J. Kaden, M. Keller,
C. Schwitzke, R. Koch, H.-J. Bauer
Institut für Thermische Strömungsmaschinen (ITS),
Karlsruher Institut für Technologie (KIT), Germany
simon.holz@kit.edu

Abstract

Smoothed Particles Hydrodynamics (SPH) simulations of the primary breakup process have been conducted using a planar prefilming airblast atomizer geometry that has been investigated experimentally. Despite the fact that a 2D study is conducted, most of the breakup phenomena are captured by the simulations. A variation of the liquid mass flow effects the simulated air flow and spray in the same way as indicated by experimental results. Using this numerical approach new insights in the primary breakup process are obtained, which can be received only difficultly in experiments. The presence of liquid at the trailing edge of the prefilmer is quantified from a side view perspective. In addition, the influence of a variation of the liquid mass flow on the liquid film and the presence of liquid at the trailing edge are characterized. Furthermore, three different wetting modes of the trailing edge are observed: The non-wetting mode which is characterized by one film wave per breakup event as well as the unstable and stable accumulation modes which are related to two film waves per breakup event. Finally, it is demonstrated that the liquid film waves and the breakup of the ligaments are slightly decoupled by the accumulation of liquid at the trailing edge.

Introduction

Prefilming airblast atomizers are widely used in the jet engines. Hence, a detailed understanding of their atomization characteristics is the prerequisite for the development of more efficient and environment friendly combustion chambers. Several attempts have been made to investigate the atomization process of this type of atomizer experimentally [1, 2, 3]. The influences of liquid properties, geometry features like the trailing edge thickness and operating conditions on the resulting ligaments and spray have been studied. The Sauter Mean Diameter and the volume weighted droplet velocities were found to be insensitive to changes in liquid film loading [2]. Furthermore, the accumulation of liquid at the trailing edge was observed and identified to be the reason for the decoupling of the liquid film flow on the prefilmer and the disintegration of the liquid at the trailing edge. The liquid accumulation was characterized in the experiment using high speed imagery from a top view perspective on the prefilmer (Fig. 1) and analysing the ratio of projected area to projected perimeter. Using this approach a slight increase of this ratio with increasing film loading was found. However, the wetting behaviour of the trailing edge in a side view perspective (Fig. 1) cannot be characterized in the experiment due to limited optical access. These limitations can be overcome using a numerical approach. In a previous study [4] the influence of trailing edge thickness on the breakup frequency resulting from the droplet number in the domain and the length of the attached ligament was investigated using the Smoothed Particle Hydrodynamics (SPH) method in a 2D domain. The main objective of the present work is to investigate the wetting of the trailing edge from a side view perspective and to clarify the role of the wetting of the trailing edge concerning the decoupling of the liquid film waves and the ligament breakup. The study is based on detailed SPH simulations using a 2D domain with liquid loadings of 50, 75 and 100 mm²/s.

The paper is organized as follows. First, the numerical method, namely the Smoothed Particles Hydrodynamics (SPH) method is briefly introduced. Second, the operating conditions and the numerical domain including the boundary conditions are discussed. Third, the investigated characteristic quantities are introduced as well as their probing positions and the analysis procedure. Fourth, the air flow field is discussed. Then, a detailed discussion of results regarding the liquid film on the prefilmer, the observed breakup phenomena, the presence of liquid at the trailing edge and the spray is given. Moreover, the interaction of liquid film flow, liquid at the trailing edge and breakup is discussed. Finally, a conclusion of the findings of the present work is given.

*Corresponding author: simon.holz@kit.edu

Numerical method

The atomization process is simulated from first principles using the Smoothed Particle Hydrodynamics (SPH) method. As the SPH method is a Lagrangian, mesh-free method, the simulation domain is discretized by particles which are convected through the domain. Hence, the particles represent the local properties of the flow like mass, momentum and energy. Due to the Lagrangian nature of the SPH method, the phase interphase is resolved directly. Neither the reconstruction of the phase interface nor a threshold for the volume fraction [1] are necessary. The diffusion of the phase interface, which is a common drawback of Volume of Fluid methods, is avoided intrinsically. A particle based formulation of the Navier-Stokes equations is solved by the SPH method. In this formulation a weighting function is used to represent the influence of the neighbouring particles on the center particle [5]. Besides the Navier-Stokes equations, models for the effect of surface tension (Continuum Surface Force method [6, 7, 8]) and the contact angle at liquid-wall interphases [9] are included. Finally, the Tait equation of state [5] is used to close the system of equations, and a background pressure is added within the Tait equation of state to improve particle arrangement.

Numerical setup

In Figure 1 the prefilmer geometry which was investigated experimentally [1, 2] is depicted as well as the corresponding computational domain of the SPH simulations to be presented within this paper. The time and

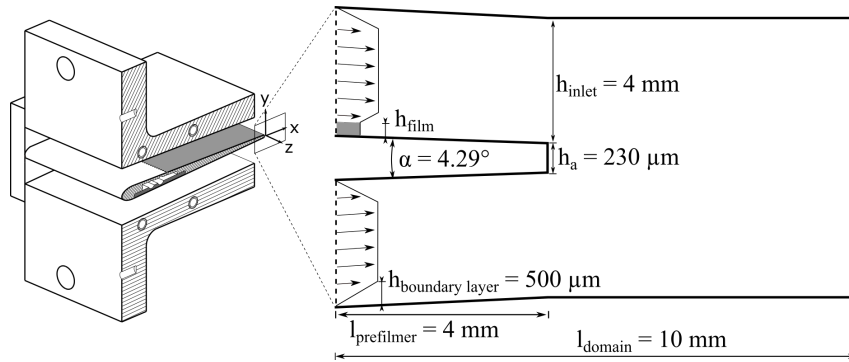


Figure 1: Prefilmer geometry (left) and corresponding computational domain (right), adopted from [5]

length scales of the atomization process cover several order of magnitude. Hence, a fine spatial discretization is required to resolve the atomization process accurately. In order to limit the numerical effort, a 2D representation of the region around the trailing edge of the prefilmer was chosen as computational domain. All geometrical properties are identical throughout this study. The air enters the computational domain above and below the prefilmer from the left hand side. The bulk velocity is set to $u_{\text{bulk}} = 50 \text{ m/s}$ and a linear velocity gradient is imposed within the boundary layer. The dashed line on the right hand side represents the outlet and the black lines are wall boundaries. The air is at ambient pressure ($p_g = 0.1 \text{ MPa}$) and temperature ($T_g = 293 \text{ K}$) with $\rho_g = 1.19 \text{ kg/m}^3$ and $\mu_g = 18.22 \times 10^{-6} \text{ kg/m}\cdot\text{s}$. Shellsol D70 is used as fuel surrogate [1, 2]. The liquid properties are: $\rho_l = 770 \text{ kg/m}^3$, $\sigma = 0.0275 \text{ kg/s}^2$ and $\mu_l = 0.00156 \text{ kg/m}\cdot\text{s}$.

The loading of the liquid film \dot{V}/b is varied from 50 to 100 mm^2/s as listed in Table 1. Due to the small computational domain, the film height h_{film} and the film velocity u_{film} have to be defined a priori at the inlet in accordance with the selected film loading. As the film height near the trailing edge is not known from experiments, a reasonable estimate must be made. Similar to the numerical investigations by Warnecke et al. [1], the film height corresponding to a film loading of $\dot{V}/b = 50 \text{ mm}^2/\text{s}$ is chosen to be $h_{\text{film}} = 100 \mu\text{m}$ (case 1). A relation between h_{film} and \dot{V}/b can be derived under the assumption of constant shear stress between the gaseous and liquid phase. Experiments by Schober [10] revealed that for an accelerated gas flow the shear stress between the gaseous and liquid phase is independent of the film loading for $\dot{V}/b \geq 40 \text{ mm}^2/\text{s}$. Due to the increase of the boundary layer thickness over the prefilmer length and the constant channel height, the gas flow is continuously accelerated. Hence, the assumption of constant shear stress is valid for the cases presented in Table 1.

Table 1: Operating conditions

case	\dot{V}/b	h_{film}	u_{film}
1	50	100.0	0.500
2	75	122.5	0.610
3	100	142.5	0.700
4	50	80.0	0.625
Unit	mm^2/s	μm	m/s

The relation between film loading and film height is derived from the Navier-Stokes equations [11]. The local velocity within the liquid film driven by an air flow is given by:

$$u_{\text{film}}(y) = \left(\left(\frac{dp}{dx} - \rho g \sin \gamma \right) \left(\frac{y}{2} - h_{\text{film}} \right) + \tau_{g,1} \right) \frac{y}{\mu_l} \quad (1)$$

Integrating the local velocity over the film height and neglecting pressure gradients in flow direction and gravitational effects, the mean film velocity is derived:

$$\bar{u}_{\text{film}} = \frac{1}{h_{\text{film}}} \int_0^{h_{\text{film}}} u_{\text{film}}(y) dy = \frac{h_{\text{film}} \tau_{g,1}}{2 \mu_l} \quad (2)$$

Assuming a constant shear force at the interface of the gas to liquid the following relation between film loading and film height is derived:

$$h_{\text{film},2} = h_{\text{film},1} \sqrt{\frac{(\dot{V}/b)_2}{(\dot{V}/b)_1}} \quad \text{with } \tau_{g,1,1} = \tau_{g,1,2} \quad \text{and } \dot{V}/b = h_{\text{film}} \bar{u}_{\text{film}} \quad (3)$$

The film heights for cases 2 and 3 are determined using this relation as well as the film loading and film height of case 1. Moreover, case 4 is set up to study the influence of the film height at constant film loading. The inlet velocities of the liquid film u_{film} are determined from the film loading.

Three different types of particles are used to discretize the walls, the air and the liquid in the computational domain (Fig. 1). The mean particle size is $dx = 2.5 \mu\text{m}$, representing the spatial discretization width. This high spatial resolution results into 13.45 Mio particles in the domain. An adaptive time stepping leads to mean time steps from $6.07 - 6.15 \cdot 10^{-9} \text{s}$. A turbulence model is not applied. An estimation of the smallest turbulent scales in time and space (Kolmogorov) revealed, that the presented predictions are actually a Direct Numerical Simulation (DNS). Using 1000 CPUs for 72 h, the simulated time covers between 181 and 191 through flow times.

Characteristic quantities and analysis procedure

This work aims to identify the relevant dynamic mechanisms of planar prefilming airblast atomizers and to clarify the role of the wetting of the trailing edge with focus on the interaction of the liquid film waves and the ligament breakup. Hence, the film height, the wetted height and area at the trailing edge, the diameter, axial position and axial velocity of the resulting droplets as well as the frequencies of the vortex shedding, the film waves and the breakup are analysed. The procedure to obtain these quantities is as follows:

The vortex shedding frequency is obtained from the time history of the axial air velocity u recorded at $x = 0.5 \text{ mm}$ and $y = -0.27 \text{ mm}$ (purple x in Fig. 2) using a Discrete Fourier Transformation (DFT).

The film height is extracted 1 mm upstream the trailing edge (Fig. 2 Detail film flow). The region covered by the green square is displayed in Fig. 3. The extracted film height corresponds to the distance of the uppermost liquid particle within the black rectangle a to the wall particles (black dots).

The presence of liquid at the trailing edge (Fig. 2 Detail trailing edge) is quantified by its probability, the wetted height h_w and the wetted area A_w . In Fig. 4 the region close to the trailing edge is depicted (yellow square). Wall particles are coloured in black and liquid particles in blue. The air particles are not depicted. The wetted height h_w is defined as the distance from the upper end of the trailing edge to the lowest liquid particle within the dashed rectangle.

In addition, the liquid within a region downstream the trailing edge confined by a square $h_a \times h_a$ (dotted square) is analysed. The wetted area A_w is equal to the area covered by the liquid in this square.

The following analysis procedure is used to obtain the spray data. A cluster detection algorithm [4] is applied to identify the SPH particles forming a droplet. A minimum number of five SPH particles is required for a droplet to be taken into account. Droplets upstream the trailing edge or attached to the lower or upper wall (Fig. 1) are neglected.

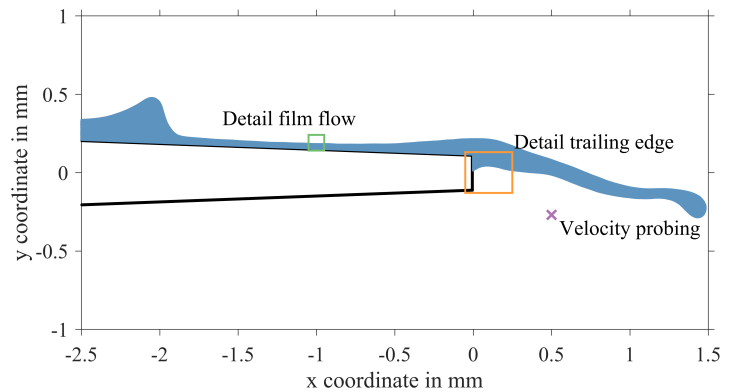


Figure 2: Probing of air velocity and overview

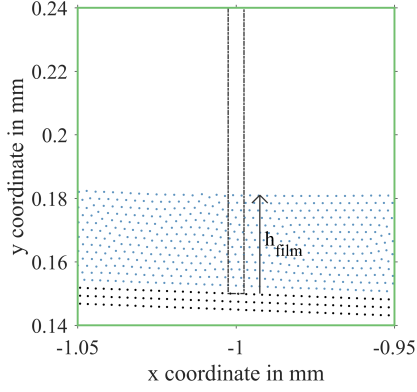


Figure 3: Detail film flow: Probing of film height

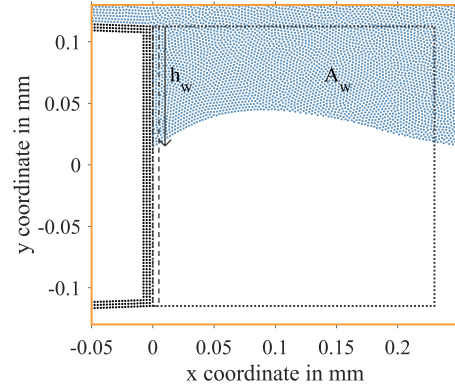


Figure 4: Detail trailing edge: Wetted height and area

Very distorted droplets are not considered to ensure the comparability to the experiment. An arbitrarily oriented minimum bounding box is fitted around the droplet. The distortion is analysed using the ratio of the smallest to longest edge length of the bounding box r_{BB} . All droplets with $r_{BB} < 0.5$ are not considered.

The area of a droplet $A_{droplet}$ is determined from the number of particles $n_{particles}$ forming the droplet. This area is assumed to be equal to the area of a circle. Hence, the droplet diameter D is given by:

$$D = \sqrt{\frac{4 A_{droplet}}{\pi}} = 2 dx \sqrt{\frac{n_{particles}}{\pi}} \quad \text{with} \quad A_{droplet} = n_{particles} dx^2 \quad (4)$$

The position and velocity of a droplet are obtained by the mean values of all SPH particles representing a single droplet. The different cases are compared using the Sauter Mean Diameter (SMD) as well as volume weighted axial positions and velocities. The experimental spray data is obtained from high speed images using a particle tracking algorithm [1].

The interaction of the film waves and the ligament breakup is studied using characteristic time scales of these phenomena. In the upper part of Fig. 5 the time record of the film height 1 mm upstream the trailing edge is depicted. The peaks in film height (yellow squares) indicate the film wave crests. The mean time between the peaks is assumed to be a characteristic time scale for the wave structure. The number of droplets within the computational domain is displayed over the simulated physical time in Fig. 5 (lower part). Please note, that the very distorted droplets, which are excluded for the spray analysis, are included for this temporal analysis. Between two subsequent breakup events no droplets are present in the domain and during a breakup event multiple local maxima in droplet number can occur (dashed circle). The following algorithm is applied to ensure that the time corresponding to a breakup event is chosen well. Each SPH particle entering the computational domain gets a unique identifier. Hence, a droplet can be linked to the time steps of its existence and tracked through the domain. At the time of the first local maximum a sample of droplets is present in the domain. First, the time when these droplets have left the domain is derived using the unique identifiers. Second, the next local maximum in droplet number is searched starting from the time when all droplets have left the domain. Third, the algorithm continues with the first step. This way all local maxima in droplet number that represent a breakup event are obtained (red triangles in the lower part of Fig. 5). The characteristic breakup time is determined by the mean time between these local maxima. Finally, frequencies for the film waves and the droplet number are derived based on the mean times between the peaks.

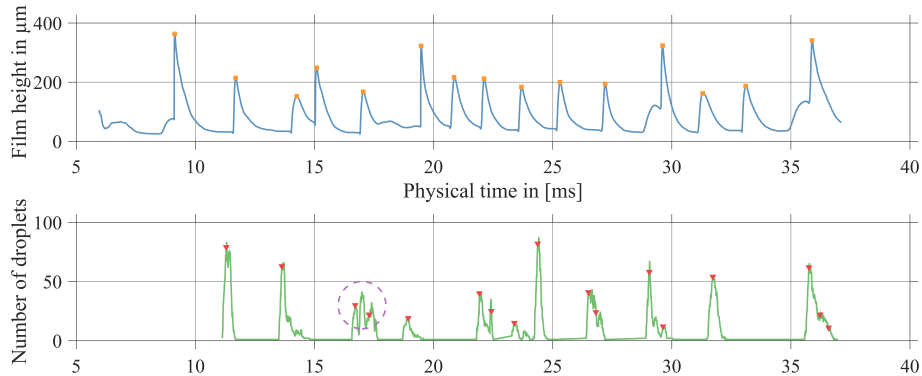


Figure 5: Frequency extraction (case 1)

Air flow field

The predicted instantaneous and time averaged air flow field of case 1 is presented in Fig. 6. Vortex shedding occurs downstream the trailing edge (Fig. 6a). The time averaged air flow field (Fig. 6b) is almost symmetric and shows a slight influence of the liquid film on the boundary layer on top of the prefilmer. Vortex shedding frequencies are extracted using DFT of the axial air velocity (Fig. 2). When the film height at the inlet is increased, the vortex frequency f_{vortex} is decreasing slightly from 11.15 kHz to 10.28 kHz. The resulting Strouhal numbers ($St = f_{\text{vortex}} h_a / u_{\text{bulk}}$) are in the range of 0.047 to 0.051, which is a quarter of the commonly observed Strouhal number of $St = 0.2$ for pure air flows. Presumably, this is caused by the detachment of the ligaments.

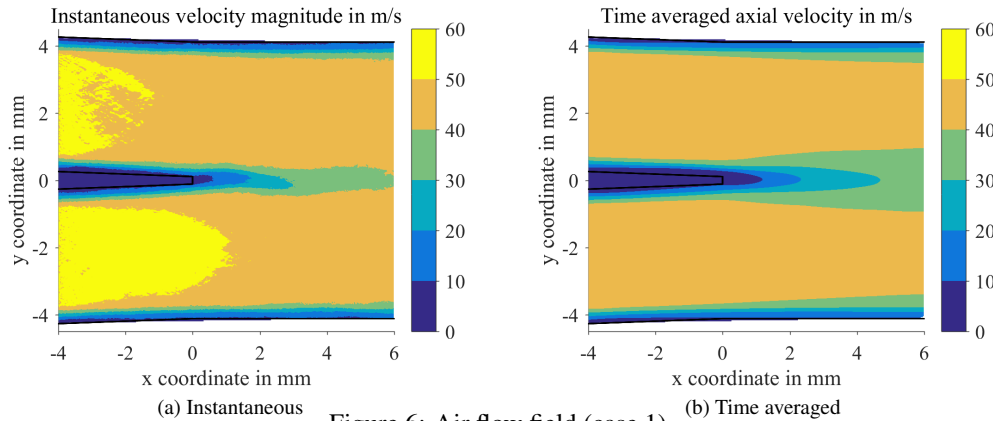


Figure 6: Air flow field (case 1)

Liquid film

The temporal mean film height on the prefilmer is depicted in Fig. 7 for different inlet film heights. For inlet film heights greater 80 μm , the film heights established on the prefilmer are smaller than the film heights at the inlet. Due to the momentum exchange between the fast air flow and the slow liquid flow the liquid is accelerated. Hence, the conservation of mass as well as the formation of film waves enforce the decrease of the film height. The initial film heights of 80 and 100 μm both represent the same film loading. As their resulting mean film height on the prefilmer is quasi identical, the robustness of the chosen way to set the initial conditions for the liquid film is demonstrated.

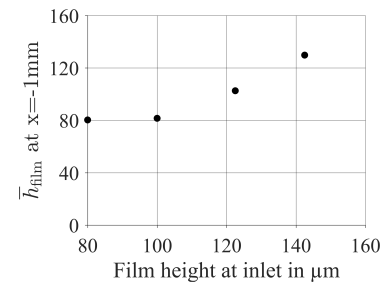


Figure 7: Film heights at $x = -1$ mm

Phenomena observed during breakup

Five subsequent snapshots of a single breakup sequence are depicted in Fig. 8 in different colors. Due to the different time scales of the breakup, the time increment between the snapshots varies. For the sake of clarity, the gaseous phase is not shown. Due to the momentum exchange from the fast gaseous phase to the slow liquid phase, waves appear on the film (i) which move to the trailing edge (ii). In case of a non-wetted trailing edge, the liquid volume advected by the wave may be trapped at the trailing edge (1st snapshot). Non-wetted trailing edges occur after breakup events where all the liquid attached to the trailing edge is transformed into a ligament and finally atomized. Wetted trailing edges usually result from previous breakup events if not all the liquid has been atomized. Sometimes, when a wave has less momentum, the liquid slowly moves from the prefilmer to the trailing edge. When a wave reaches the trailing edge, a crest is formed (1st snapshot) and then elongated into a ligament (see (iii) and 2nd snapshot). Within the process of elongation, the ligament is fed by the liquid available on the prefilmer and from the liquid already attached to the trailing edge. The crest of the ligament starts to form an elevation at

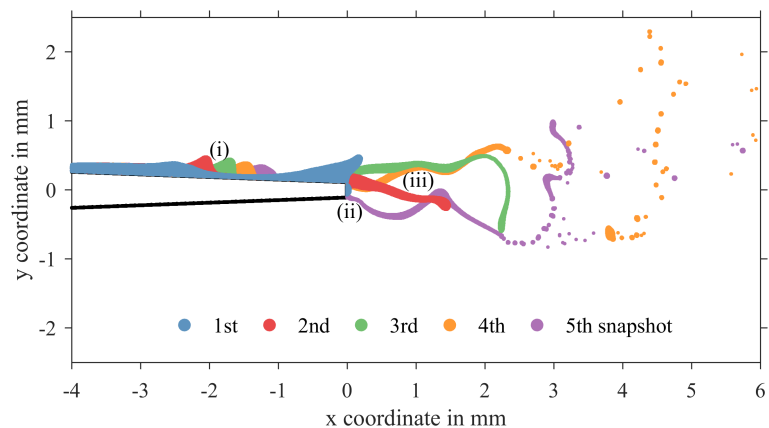


Figure 8: Five subsequent snapshots of one breakup sequence (case 1)

the trailing edge, which is exposed to the high speed airflow. Consequently, the ligament is elongated and bend to a c-shape structure (3rd snapshot). This shape is similar to the liquid bags as they occur in the experiment. These liquid bags consist of a thick rim and a thin interior film. Hence, a finer spray is produced in reality compared to the 2D simulations. However, as the shear force imposed by the air flow to the liquid overcomes the surface tension, a part of the ligament is detached (4th snapshot). The part of the ligament which is still attached to the trailing edge is pushed downwards by the high speed airflow (5th snapshot) and fully separates from the trailing edge due to its heigh momentum. This movement of the ligament mostly occurs from top to bottom and is called flapping. All the phenomena described previously are involved in the primary breakup. In addition, the subsequent disintegration of large liquid structures into smaller droplets (secondary breakup) can be observed in the 4th and 5th snapshot. All described observations are in good qualitative agreement with experiments [1, 3]. Due to the 2D nature of the presented SPH simulations, transversal film waves and the formation of liquid bags with a thick rim and a thin interior film cannot be reproduced.

Presence of liquid at the trailing edge

Three different wetting modes of the trailing edge are depicted in Fig. 9. Due to the 2D nature of the predictions the waves reaching the trailing edge can be clearly distinguished. The non-wetting mode (Fig. 9a) is

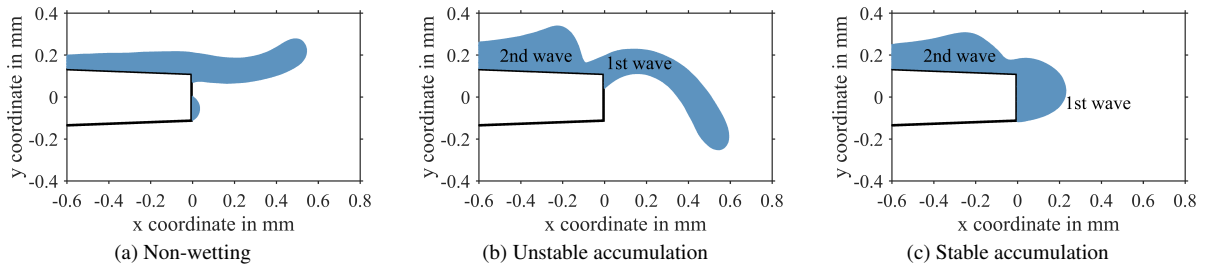


Figure 9: Wetting modes of trailing edge (case 1)

characterized by a single wave that is directly converted into a ligament wetting the trailing edge only slightly. Another observed mode is called unstable accumulation (Fig. 9b). Here, a first wave reaches the trailing edge and forms a new ligament. While the ligament (1st wave) is elongated, another wave (2nd wave) reaches the trailing edge. The liquid of the incoming wave directly feeds the elongating ligament and boosts the breakup due to the additional momentum. The stable accumulation mode (Fig. 9c) starts with a wave moving from the prefilmer to the trailing edge (1st wave) wetting the whole trailing edge and forming a semicircle shape. This liquid accumulation remains stable until the next wave (2nd wave) reaches the trailing edge which leads to a final destabilization of the accumulation. Consequently, the liquid of the first and the second wave will detach at once. The three wetting modes can be characterized by the number of involved film waves. The non-wetting mode is triggered by a single wave, whereas the unstable and stable accumulations modes are characterized by the breakup of the liquid of two subsequent film waves. Hence, the former mode represents a strong coupling between the film waves and the breakup whereas the latter modes constitute a slight decoupling.

The position and size of the liquid accumulation at the trailing edge can be characterized qualitatively by considering the presence probability of liquid near the trailing edge (Fig. 4 dotted square). In Fig. 10 the presence probability of the liquid within the dotted square is depicted for case 1. The most wetted area is in the upper part of the trailing edge, indicating that most of the ligaments are connected to the liquid film on the prefilmer during their elongation and breakup. Slight convex contours can be observed in Fig. 10. They represent larger liquid accumulations. The position and size of the liquid accumulation can be characterized quantitatively using temporal mean values of the wetted height h_w and area A_w (Fig. 4). The normalized values are depicted in Fig. 11. About

57% of the trailing edge are wetted on average. A normalized wetted height of $\bar{h}_w/h_a = 60\%$ is related to $y = -23\mu\text{m}$, which represents the most wetted area discussed previously. The normalized wetted height is insensitive to changes of film

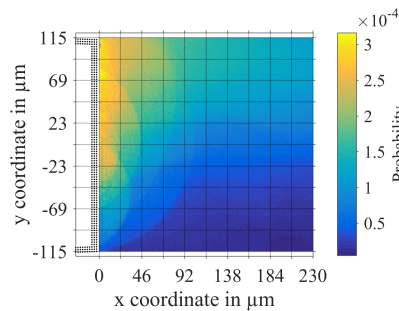


Figure 10: Liquid at trailing edge (case 1)

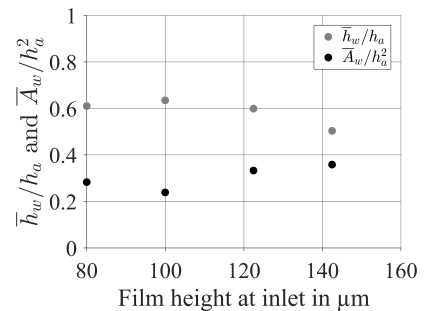


Figure 11: Characteristic wetting ratios

height as well as of the film loading. The average covering of the square h_a^2 by liquid is about 30 %. No clear effects of \bar{A}_w/h_a^2 on the film height or film loading can be observed. The insensitivity of both quantities indicate, that the frequency of all three wetting modes is independent of both film height and film loading.

Spray characteristics

The droplets resulting from the ligament breakup are characterized by their diameter, axial position and velocity. In Fig. 12 bivariate histograms of droplet diameter, axial velocity and position obtained from the simulations as well as the experiment are depicted for case 1. The colours represent the relative number of events. Fig. 12a and 12b illustrate how the droplets are accelerated from their origin to the end of the domain. Both,

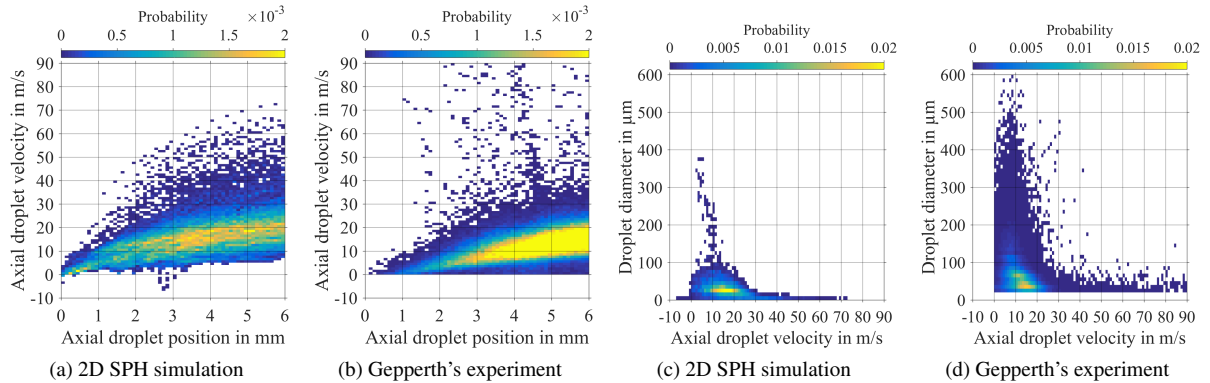


Figure 12: Interdependencies of droplet diameter, axial velocity and position (case 1)

experiment and simulation show similar contours. This is an indicator that the 2D SPH simulations reproduce the physics of the experiment quite well. The relation between droplet diameter and axial velocity is depicted in Fig. 12c and 12d. The drop sizes obtained by the simulation are significantly smaller than in the experiment. Duan et al. [12] found that the critical Weber number in 2D simulations was smaller than in 3D experiments at the same relative velocity. Hence, it is reasonable that the droplets generated by the 2D simulations are smaller than those of the 3D experiment. Nevertheless, the principal dependencies are similar in simulation and experiment.

In addition, Sauter Mean Diameters (SMD), volume weighted axial positions \bar{x}_V and velocities \bar{u}_V have been derived for all four cases and three experimentally investigated operating points (Table 2). In the experiment these three characteristic values are strongly independent from the film loading. A similar behaviour can be observed for the SPH simulations (cases 1 - 4). The difference of the experimental SMDs and the SMDs obtained from the SPH simulations results from the 2D nature of the simulations. This affects also the ligament length and consequently the volume weighted axial positions obtained from the 2D simulations resulting in smaller values than in the experiment. The volume weighted axial velocities from the simulations are 17 to 20 % smaller than in the experiment, which is a good agreement considering the limited spatial dimension of the numerical domain. In summary, the spray characteristics obtained by 2D SPH simulations reflect the interdependencies between droplet diameter, position and velocity of the experiment and their independence from the liquid film loading quite well.

Table 2: Spray characteristics

case	\dot{V}/b	h_{film}	SMD	\bar{x}_V	\bar{u}_V
Exp.	25	-	164	3.9	8.5
Exp.	50	-	166	4.3	8.7
Exp.	75	-	162	4.5	8.6
1	50	100.0	124	2.8	7.0
2	75	122.5	123	2.8	7.1
3	100	142.5	116	3.3	8.1
4	50	80.0	138	3.1	7.1
Unit	mm ² /s	μm	μm	mm	m/s

Interaction of film flow, liquid accumulation at the trailing edge and ligament breakup

Five different dynamic mechanisms can be identified in the context of planar prefilming airblast atomizers: the vortex shedding of the air, the film waves, the accumulation of liquid at the trailing edge as well as the flapping and breakup of ligaments. Within this study only the frequency of the film waves and the frequency of ligament breakup will be analysed (Fig. 5). The vortex shedding frequencies (11.15 – 10.7 kHz) are one order of magnitude larger than the film and breakup frequencies. The temporal dynamics of the wetted height h_w and area A_w which quantify the liquid accumulated at the trailing edge do not have a clear regular temporal pattern. Hence, no characteristic time scale or frequency of the liquid accumulation can be determined. The ligament flapping is part of the ligament breakup as it takes place once for most breakup events. The characteristic frequencies of the film waves

and the ligament breakup are depicted in Fig. 13. Both frequencies strongly depend on the film loading (Table 2). The wave frequency is for all four cases larger than the breakup frequency. This indicates that more film waves than ligament breakup events occur. On average 1.08 – 1.15 film waves occur per breakup event. This observation is in good agreement with the previously discussed wetting modes of the trailing edge (Fig. 9). Furthermore, this is an indicator that the non-wetting mode (one film wave per breakup event) occurs more often than the unstable and stable accumulation modes (two film waves per breakup event). Hence, the liquid film waves and the breakup of the ligaments are slightly decoupled by the accumulation of liquid at the trailing edge.

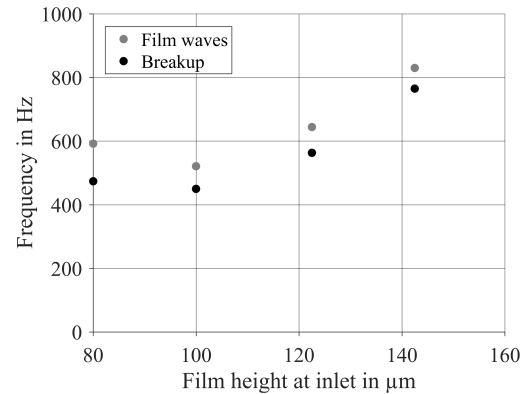


Figure 13: Frequencies of film waves and breakup

Summary and Conclusions

In the present work 2D SPH simulations of the experimentally well investigated planar prefilming airblast atomizer of Gepperth have been presented. It has been demonstrated that, although the simulations are 2D, many breakup phenomena can be captured by the simulations. Furthermore, it was found that the sprays of the experiment and the simulations match qualitatively. New insights into the primary breakup process of planar prefilming airblast atomizers have been obtained. The presence of liquid at the trailing edge of the prefilmer has been quantified from a side view perspective. In addition, the influence of a variation of the liquid mass flow on the liquid film and the presence of liquid at the trailing edge have been characterized. Furthermore, three different wetting modes of the trailing edge have been observed: The non-wetting mode which is characterized by one film wave per breakup event as well as the unstable and stable accumulation modes which are related to two film waves per breakup event. Finally, it has been demonstrated that the liquid film waves and the breakup of the ligaments are slightly decoupled by the accumulation of liquid at the trailing edge. These findings and the possibility to simulate the atomization process from first principles, foster the development of primary atomization models.

Acknowledgements

The numerical computations were performed on the high performance super computing cluster ForHLR (Phase I) at the Karlsruhe Institute of Technology (KIT), Karlsruhe, Germany. The computer cluster was funded by the Ministry of Science, Research and the Arts Baden-Württemberg and the DFG ("Deutsche Forschungsgemeinschaft") within the framework program bwHPC. Furthermore, the funding by the German aeronautical research program LuFo V within the project EmKoTec is gratefully acknowledged.

References

- [1] Warncke, K., Gepperth, S., Sauer, B., Sadiki, A., Janicka, J., Koch, R. and Bauer, H.-J., *International Journal of Multiphase Flow*, 91:208 – 224 (2017).
- [2] Gepperth, S., Müller, A., Koch, R. and Bauer, H.-J., *ICLASS, 12th Triennial International Annual Conference on Liquid Atomization and Spray Systems*, Heidelberg, Germany (2012).
- [3] Inamura, T., Shirota, M., Tsushima, M., Kato, M., Hamajima, S. and Sato, A., *ICLASS, 12th Triennial International Annual Conference on Liquid Atomization and Spray Systems*, Heidelberg, Germany (2012).
- [4] Braun, S., Wieth, L., Koch, R. and Bauer, H.-J., *ICLASS, 13th Triennial International Conference on Liquid Atomization and Spray System*, Tainan, Taiwan (2015).
- [5] Braun, S., Koch, R. and Bauer, H.-J., *High Performance Computing in Science and Engineering '16*, pp. 321–336, Springer Nature (2016).
- [6] Brackbill, J., Kothe, D. and Zemach, C., *Journal of Computational Physics*, 100(2):335–354 (1992).
- [7] Morris, J. P., *International Journal for Numerical Methods in Fluids*, 33(3):333–353 (2000).
- [8] Adami, S., Hu, X. and Adams, N., *Journal of Computational Physics*, 229:5011–5021 (2010).
- [9] Wieth, L., Braun, S., Koch, R. and Bauer, H.-J., *ILASS Europe, 26th Annual Conference on Liquid Atomization and Spray Systems*, Bremen, Germany (2014).
- [10] Schober, P., *Berührungsfreie Erfassung beschleunigter schubspannungsgetriebener Kraftstoffwandfilme unter Druckeinfluss*, Ph.D. thesis, Institut für Thermische Strömungsmaschinen, Universität Karlsruhe (2009).
- [11] Chaussonnet, G., Riber, E., Vermorel, O., Cuenot, B., Gepperth, S., Koch, R., *ILASS Europe, 25th Annual Conference on Liquid Atomization and Spray Systems*, Chania, Greece (2013).
- [12] Duan, R.-Q., Koshizuka, S., Oka, Y. *Nuclear Engineering and Design*, 225:37–48 (2003).